An Analysis of the Formation of Interconnecting Loops

**Jie Chen · Henrik Lundstedt · Yuanyong Deng ·
Peter Wintoft · Yin Zhang**

Abstract Fifty interconnecting loops (ILs) that are induced by new-born active regions are
investigated. The formation period of four ILs including two same-hemisphere intercon-
necting loops (HILs) and two transequatorial loops (TLs) are analyzed. The magnetic flux
related with these loops is studied. Considering the active region pairs related with the IL
as a magnetic system, the total magnetic flux has a tendency of increasing for this system,
the signs of net magnetic flux tend to be opposite for the active region pairs. There is no
difference between HILs and TLs in this aspect.

Keywords Active region · Magnetic field · Coronal loop

1. Introduction

Soft X-ray images have revealed that active regions sometimes are connected to each other
by coronal loops much larger than active-region structures on the Sun (Chase *et al.*, 1976;
Švestka and Howard, 1981; Fárník, Karlický, and Švestka, 1999; Pevtsov, 2000; Khan and
Hudson, 2000; Wang *et al.*, 2006, 2007; Harra *et al.*, 2007). We call this type of coronal
loop an interconnecting loop (IL). Some large-scale coronal loops are observed to join ac-
tive regions in the same hemisphere, and we call them hemispheric interconnecting loops
(HIL); others are observed to connect active regions across the Equator, which are called
transequatorial loops (TL).

There are two basic explanations of the formation of transequatorial loops: One is the
formation of a TL generated by magnetic reconnection. Tsuneta (1996) demonstrated an
X-type TL formed by reconnection. Later, Fárník, Karlický, and Švestka (1999) found that

J. Chen (✉) · Y. Deng · Y. Zhang
Key Laboratory of Solar Activity, National Astronomical Observatories, Chinese Academy of Science,
Datun Road A20, Chaoyang District, 100012, Beijing, China
e-mail: chenjie@bao.ac.cn

J. Chen · H. Lundstedt · P. Wintoft
Swedish Institute of Space Physics, Scheelev. 17, 22370, Lund, Sweden

TLs originate from the two active regions toward and across the Equator through reconnection. They suggested that this reconnection is caused by differential rotation. Yokoyama and Masuda (2009) analyzed a TL generated through magnetic reconnection that occurred between weak magnetic fields of coronal holes and strong magnetic fields of active regions. The other type is a TL formed through emergence of sub-photospheric magnetic fields. This explanation was provided by Jiang, Choudhary, and Wang (2007) using a numerical simulation of a solar-dynamo model. Švestka and Howard (1981) explained the formation of interconnecting loops in another way: They found cases when the magnetic loops existed prior to the brightening and showed an example of a slow brightening of a pre-existing loop.

Flux emergence is considered as an important trigger of solar activity. Martin *et al.* (1982) studied 88 flares and found that two-thirds of these flares were closely related to flux emergence. Feynman and Martin (1995) found the quiescent-filament-associated CMEs occurred after new flux emergence. Lara, Gopalswamy, and DeForest (2000) showed that flare-associated CMEs occurred during the maximum phase of magnetic-flux emergence. Zhang, Zhang, and Zhang (2008) made a statistical study about the relationship between flux emergence and CME eruption, the results showed that the relation is complex and that the appearance of flux emergence alone is not unique for the initiation of a CME eruption.

For an active region, the magnetic flux in the leading and following polarities is often not balanced. The magnetic-flux imbalance of the Sun was studied by Choudhary, Venkatakrishnan, and Gosain (2002) using longitudinal magnetograms. The results showed that the $10°$ to $40°$ active latitude zone in the individual hemispheres during the solar maximum had a flux imbalance of more than 20%, which is reduced to below 10% when the entire Sun is considered. Green *et al.* (2003) investigated four cases with emerging flux and showed that the long-term imbalance is related to the East–West distance from the central meridian, but the imbalance is not persistent.

The hemispheric interconnecting loops and transequatorial loops are large-scale structures; are there differences between them? Considering the magnetic flux of the two active regions connected with interconnecting loops, we calculate the magnetic-flux variation in the system during the formation of ILs. The magnetic flux of 50 ILs are calculated, four interconnecting loops including two HILs and two TLs are analyzed. In Section 2 we introduce the data analysis. In Section 3, cases are described, and statistical results are shown. The conclusion and discussion are presented in Section 4.

2. Data Reduction

2.1. MDI

The MDI instrument (Scherrer *et al.*, 1995) computes the magnetic signal onboard the SOHO spacecraft by differencing Dopplergrams obtained in right- and left-circular polarized light. The magnetograms are recorded by a 1024×1024 CCD detector with a pixel size of $2''$. There are two kinds of MDI full-disk magnetogram data: one-minute cadence data and 96-minute cadence data. The recalibrated level 1.8.2 and 96-minute cadence data are used. The new calibration uses an improved sensitivity flat-field map for the magnetic field. Pixels with obvious cosmic-ray contamination have been removed.

The processes are carried out to co-align the images, remove differential rotation effects, and make geometric correction. We choose the related active regions in MDI time-series images; these images taken at different times are aligned based on the nonlinear mapping defined by the differential solar rotation (Howard, Harvey, and Forgach, 1990),

$$\omega' = 2.894 - 0.428 \sin^2 b - 0.370 \sin^4 b \ \mu\text{rad s}^{-1}, \tag{1}$$

Figure 1 The data-reduction
processes of MDI images.

| Series MDI full-disk images |

| Choose an active region and coalign |

| Remove differential rotation effects |

| Transform the image from pixel to arcsecs |

| Geometric correction |

get

| Data which are needed |
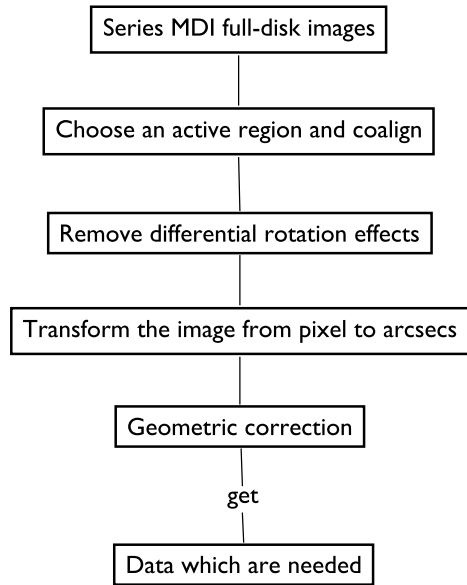
where b is the latitude. ω' is the sidereal rotation rate. The synodic rotation rate is obtained
by

$$\omega = \omega' \times 10^{-6} \times 3600 \times 24 - 0.9856 \ \mathrm{rad\,day}^{-1}. \tag{2}$$

Then we transform the image from pixels to arcsecs through interpolating the selected
region to $1'' \times 1''$ resolution. If an observed area is away from disk center, the observed
area becomes shortened. The image should be transformed to heliographic coordinates. The
calculation of the heliocentric angle $[\psi]$ uses the following formula:

$$\cos \psi = \sin b \sin b_0 + \cos b \cos b_0 \cos(l - l_0), \tag{3}$$

where b_0 and l_0 represent the heliographic latitude and longitude of the disk center. The areas
are corrected by dividing by $\cos \psi$. This effect is automatically corrected when rotational
mapping to the central meridian is applied. The data less than ten Gauss are considered to
be noise and are set to zero. The procedure is shown in Figure 1.

Magnetic flux of the two active regions that are related by the interconnecting loops are
considered. Two parameters are calculated about the active regions: net magnetic flux and
total magnetic flux:

$$\Phi_{\mathrm{net}} = \sum \Phi_{\mathrm{pos}} + \sum \Phi_{\mathrm{neg}} = \sum B_{i,j} S, \tag{4}$$

$$\Phi_{\mathrm{tot}} = \sum \Phi_{\mathrm{pos}} + \left| \sum \Phi_{\mathrm{neg}} \right| = \sum |B_{i,j}| S. \tag{5}$$

i, j is the pixel position of the magnetic field, S is the area per pixel.

2.2. SXT

Soft X-ray images are taken from the *Yohkoh/Soft X-ray Telescope* (SXT: Tsuneta *et al.*,
1991). For the purpose of this study, we have considered full-disk SXT observations with

a spatial resolution of 4.9″. Data are downloaded from http://solar.physics.montana.edu/ylegacy/. The corrected and composite level-2 data which were taken using AlMg filter are selected.

For the SXT images, we can find the positions of the solar center in the header of the FITS files. This information is used to co-align solar center and image center. Then the selected regions are corrected for differential rotation and geometric effects, which is similar to the procedure described in the previous section.

3. Observations

Yohkoh/SXT data are available from 1991 to 2001. Thousands of interconnecting loops were observed by SXT. During the observations of *Yohkoh*/SXT, in order to calculate the magnetic field of active regions related with ILs, full-disk magnetograms obtained from the National Solar Observatory (NSO) at Kitt Peak and SOHO/MDI can be considered. However, there are only one or two magnetograms per day from NSO at Kitt Peak, and it is not simple to calculate the variation of magnetic fluxes of active regions. Therefore, only data from SOHO/MDI are selected. MDI provides data from 1996, and there are gaps from June to October in 1998 and from January to February in 1999. In this study, events or samples are covered through investigating the *Yohkoh*/SXT data set and SOHO/MDI data set from 1996 to 2001.

The criteria for the selected samples are as follows: First, we investigate the SXT data set since 1996, all of the events for which new active regions induced the formation of ILs are found. Second, with these events, the MDI data set is investigated. Events where both active regions existed within $\pm 50°$ are selected. Fifty interconnecting loops (ILs) which are generated by new active regions are finally selected.

When an interconnecting loop exists in one hemisphere only, it is called a hemispheric interconnecting loop (HIL). A HIL anchors two active regions in the same hemisphere. On the other hand, an IL crosses the Equator and is thus named a transequatorial loop (TL). A TL connects two active regions in opposite hemispheres.

The selected ILs are listed in Table 1. The first column shows the type of IL; the second column the formation time; the third column the old active region number; the fourth column the hemisphere that the old active region exists in; the fifth and sixth columns show the variation of Φ_{tot} and the sign of Φ_{net} for the old active region during the formation of IL; the seventh column shows the number of the new active region; the eighth and ninth columns have the same meaning as column four and column five, but for the new active regions. When the variation of Φ_{tot} is described, "↑" indicates that Φ_{tot} is increasing, "↓" indicates that Φ_{tot} is decreasing, and "?" represents Φ_{tot} is increasing at some times, but decreasing at others. Because all of the ILs are found based on the new active regions, the values of Φ_{tot} are increasing for all of the new active regions; they are not listed in this table.

3.1. Cases Analysis

In order to understand the generation process of ILs, the formation of four ILs are observed during the flux emergence in new active regions. Two hemispheric interconnecting loops (HILs) and two transequatorial loops (TLs) are included. All of them were observed by the *Yohkoh Soft X-ray Telescope* (SXT). In order to investigate the photospheric magnetic flux related to the coronal loops, the SOHO/MDI full-disk longitudinal magnetograms are also analyzed. The four ILs are listed in Table 2. The first column shows the type of the IL; the

Table 1 Interconnecting loops (ILs) and related active regions.

Type	Date	AR old	HS[a]	Φ_{tot}	Φ_{net}	AR new	HS[a]	Φ_{net}
HIL[b]	21-May-97 09:52:18	8040	N	↑	+	8045	N	+
HIL	25-Jul-97 00:24:12	8062	N	?	–	8065	N	+
HIL	30-Aug-97 01:10:02	8078	N	?	–	8080	N	+
HIL	09-Oct-97 05:22:10	8092	N	?	+	8093	N	–
HIL	08-Dec-97 17:38:47	8116	N	?	+	8119	N	–
HIL	04-Nov-98 16:18:57	8373	S	↑	–	8379	S	–
HIL	07-Dec-98 09:54:51	8402	S	?	+	8404	S	–
HIL	05-Feb-99 10:33:34	8453	S	?	–	8454	S	+
HIL	02-Mar-99 23:50:07	8478	S	↑	–	8479	S	–
TL[c]	07-Jul-99 12:41:00	8614	N	↓	+	8626	S	–
HIL	01-Aug-99 04:00:09	8648	N	↑	–	8654	N	+
HIL	02-Aug-99 09:05:54	8650	N	?	+	8656	N	+
HIL	11-Sep-99 23:22:24	8690	N	↑	+	8699	N	+
TL	28-Oct-99 05:26:34	8744	N	↓	+	8746	S	–
HIL	04-Nov-99 03:40:03	8749	S	↓	+	8752	S	–
TL	08-Nov-99 19:10:50	8754	S	?	–	8760	N	+
HIL	16-Nov-99 19:17:42	8766	N	↑	+	8768	N	+
HIL	16-Nov-99 19:17:42	8759	N	↓	–	8768	N	+
TL	16-Nov-99 01:36:02	8765	S	↑	–	8768	N	+
HIL	13-Dec-99 13:20:45	8794	S	↑	+	8797	S	–

Table 1 (*Continued*)

Type	Date	AR old	HS[a]	Φ_{tot}	Φ_{net}	AR new	HS[a]	Φ_{net}
HIL	11-Jan-00 09:52:39	8821	N	↑	–	8826	N	+
HIL	18-Jan-00 12:50:56	8831	S	↑	–	8837	S	+
HIL	24-Jan-00 13:26:29	8840	S	↓	+	8842	S	–
HIL	25-Jan-00 21:43:16	8838	N	↓	+	8844	N	+
HIL	25-Jan-00 11:59:12	8841	S	↑	+	8845	S	+
HIL	03-Mar-00 16:36:29	8891	S	↓	–	8897	S	+
HIL	07-Mar-00 08:59:48	8898	S	↑	–	8903	S	+
TL	08-Mar-00 12:40:56	8898	S	↑	–	8904	N	+
HIL	20-Mar-00 05:01:29	8910	N	↑	+	8918	N	–
HIL	20-Mar-00 05:01:29	8917	N	↑	+	8918	N	–
TL	23-Mar-00 14:59:37	8916	N	↑	+	8926	S	+
HIL	01-Apr-00 10:05:27	8941	N	?	+	8943	N	–
TL	20-Apr-00 15:02:41	8963	N	↓	+	8968	S	–
TL	29-May-00 01:18:19	9017	S	↑	–	9021	N	–
TL	19-Jun-00 19:02:46	9048	N	↑	+	9050	S	–
HIL	23-Jun-00 18:05:09	9049	S	↑	+	9058	S	–
TL	07-Aug-00 06:54:36	9114	N	↑	+	9120	S	–
HIL	02-May-01 18:29:24	9445	N	↑	–	9447	N	–
TL	05-May-01 00:39:04	9445	N	↑	–	9450	S	+
HIL	14-May-01 18:23:26	9454	N	↑	+	9459	N	+

Table 1 (*Continued*)

Type	Date	AR old	HS[a]	Φ_{tot}	Φ_{net}	AR new	HS[a]	Φ_{net}
HIL	07-Jun-01 18:48:55	9484	S	↓	–	9494	S	–
HIL	08-Jun-01 07:36:57	9488	S	?	–	9494	S	–
TL	19-Jun-01 22:24:28	9504	N	↑	+	9509	S	+
TL	20-Jun-01 16:52:46	9504	N	↑	+	9510	S	–
TL	23-Jun-01 00:47:14	9514	N	↑	–	9515	S	+
HIL	11-Jul-01 20:51:02	9537	S	↑	+	9539	S	+
TL	06-Sep-01 02:27:42	9601	N	↓	–	9609	S	–
HIL	20-Sep-01 01:44:39	9622	N	?	–	9631	N	–
HIL	11-Oct-01 06:13:27	9657	N	?	+	9660	N	–
HIL	14-Dec-01 09:42:17	9734	S	↑	+	9739	S	–

[a]Hemisphere of the related active region.

[b]Hemispheric interconnecting loop.

[c]Transequatorial loop.

Table 2 The four interconnecting loops (ILs).

[a]Magnetic polarity of the footpoint of the IL.

[b]Preceding or following polarity.

[c]Hemispheric interconnecting loop.

[d]Transequatorial loop.

Cas.	Date	AR old	MP[a] old	P/F[b]	AR new	MP new	P/F
HIL[c]	21-May-97	8040	+	F	8045	–	P
HIL	25-Jul- 97	8062	+	P	8065	–	F
TL[d]	07-Jul- 99	8614	+	P	8626	–	P
TL	20-Apr- 00	8963	+	P	8968	–	P

second column the formation date; the third and fourth columns show the old active region numbers and magnetic polarities; the fifth column shows the preceding or following polarity; the last three columns show the new active region numbers, where magnetic polarities and preceding/following polarities are listed.

3.1.1. Case 1

Figure 2 shows a hemispheric interconnecting loop (HIL) and related longitudinal magnetogram on 21 May 1997. In the left panel, the soft X-ray image observed by *Yohkoh*/SXT is
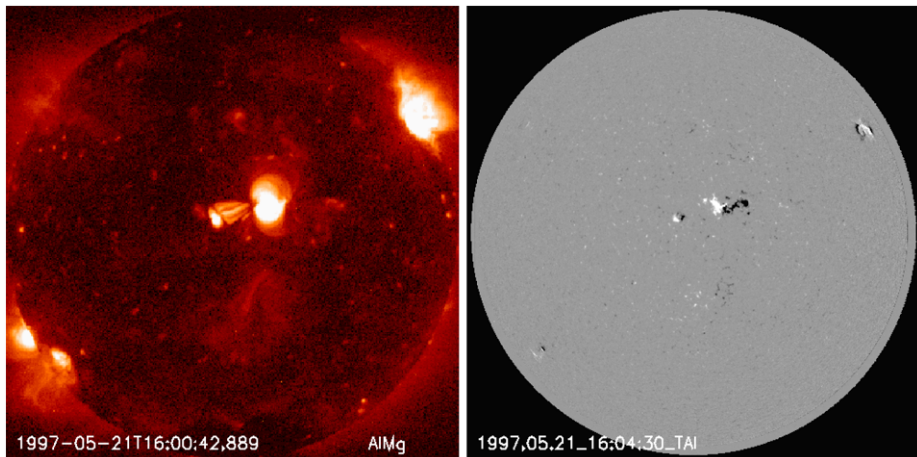
Figure 2 A hemispheric interconnecting loop on 21 May 1997. Left: *Yohkoh*/SXT image; Right: SOHO/MDI image.

shown. In the right panel, the full-disk longitudinal magnetogram observed by SOHO/MDI is shown. The HIL connects the positive polarity in AR 8040 and negative polarity in AR 8045.

The HIL formation and evolution of the related active regions are shown in Figure 3. In the top panel, the HIL formation is shown in a sequence of images. At 22:28 on 20 May, expanding structures start to form from both of the regions; at 06:42 on 21 May, a narrow loop appeared connecting the two regions; then the loop became wider and brighter. At 09:52, a clear, brightening, vivid loop was formed. The middle panel shows the evolution of AR 8045 covering the same time period of the SXT images. AR 8045 is a new simplified β-type active region. Before the narrow loop appeared, there are no clear bipolar structures. After the distinct loop formed, a clear bipolar structure was seen. Following the vivid loop, the bipolar magnetic structure persisted and the area and magnetic flux were increasing. The bottom panel shows the evolution of AR 8040. AR 8040 first appeared at N06E56 on 17 May; it is also a β-type active region.

Variations of magnetic flux in the two active regions are shown in Figure 4. The periods from the beginning to the moments of the dashed lines show the variation of magnetic flux during the formation of the HIL. The left panel shows the variation of the net and total magnetic flux for AR 8040; the right panel the corresponding flux variation in AR 8045 is plotted. From the plots, we can see that the total magnetic fluxes are increasing and they are in the increasing phases for the two active regions. During the formation of the HIL, the net magnetic flux in AR 8040 is positive, the positive magnetic flux has a weak dominance in this active region. For AR 8045, the net magnetic flux is positive and increasing, which means that the positive magnetic polarity has a preference and the positive magnetic flux increases more quickly than the negative flux.

3.1.2. Case 2

Figure 5 shows another HIL in the northern hemisphere on 25 July 1997. The two images show that the HIL connects the positive polarity in AR 8062 and negative polarity in AR 8065.
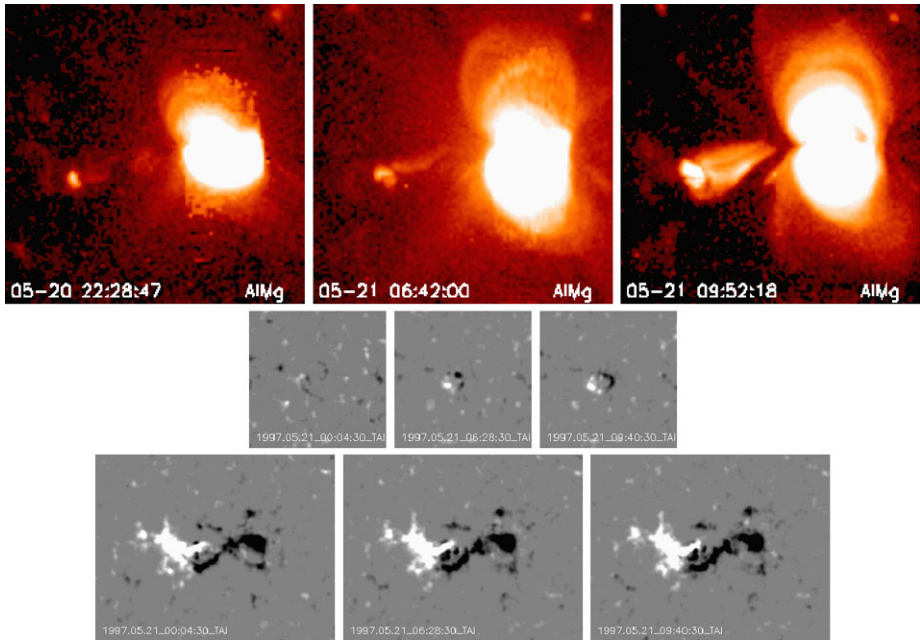
Figure 3 Formation of the HIL on 21 May 1997 and evolution of the related active regions. Top: formation process of the HIL, the field of view is $491'' \times 491''$; Middle: evolution process of AR 8045, the field of view is $100'' \times 100''$; Bottom: evolution process of AR 8040, the field of view is $180'' \times 140''$.
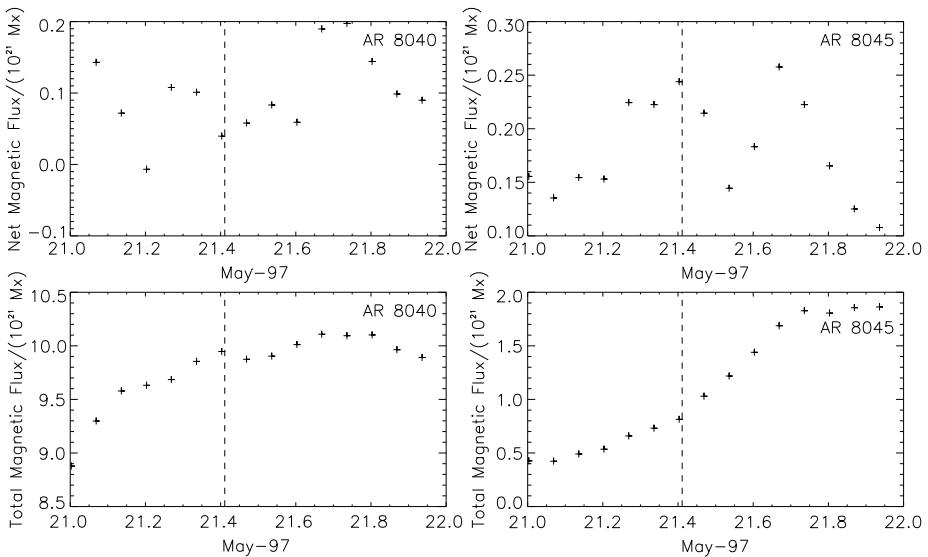

Figure 4 Variations of flux in the two active regions during the formation of the HIL, the dashed line shows the time that the HIL formed. Left panel: the variation of the AR 8040 for the net magnetic flux and total magnetic flux; Right panel: the variation of flux in AR 8045.
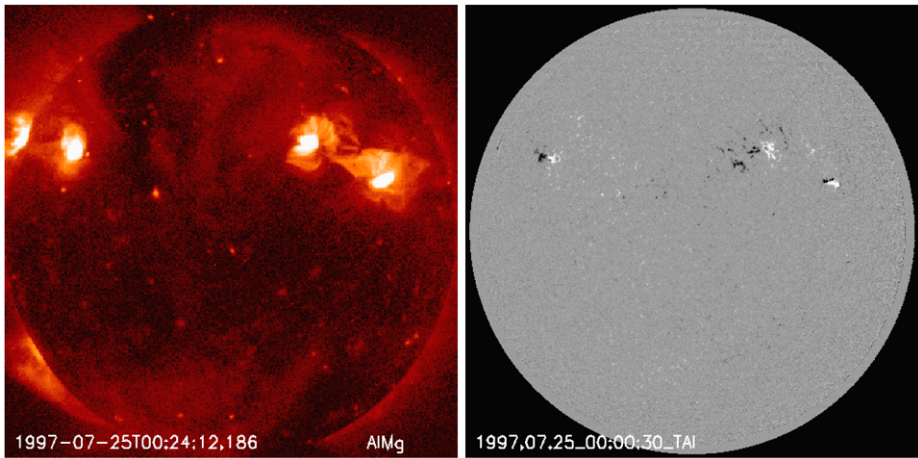
Figure 5 A hemispheric interconnecting loop on 25 July 1997. Left: *Yohkoh*/SXT image; Right: SOHO/MDI image.
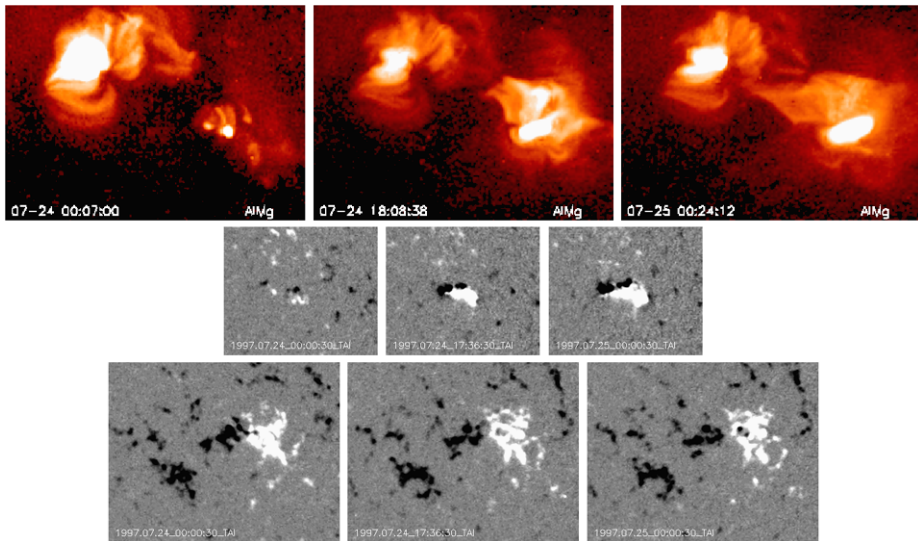
Figure 6 An interconnecting loop between AR8062 and AR8065 from 24 July 1997 to 25 July 1997. Top: formation of the HIL, the field of view is 140 pixel × 100 pixel, 1 pixel = 4.91″; Middle: evolution of AR 8065, the field of view is 120″ × 100″; Bottom: evolution of AR 8062, the field of view is 180″ × 140″.

Figure 6 demonstrates the formation of the HIL and evolution of the related active regions. The top panel shows the formation of the HIL. The middle and bottom panels show the evolution of AR 8065 and AR 8062 during the period of HIL formation. At 00:00 on 24 July, there was emerging magnetic flux in the new active region 8065; almost at the same time, the SXT image was brightening at the same region. At 17:36, MDI image showed clear bipolar structure in AR 8065 and the SXT image showed the expanding brightening from the region at 18:08. Following the growing of AR 8065, an entire interconnecting loop
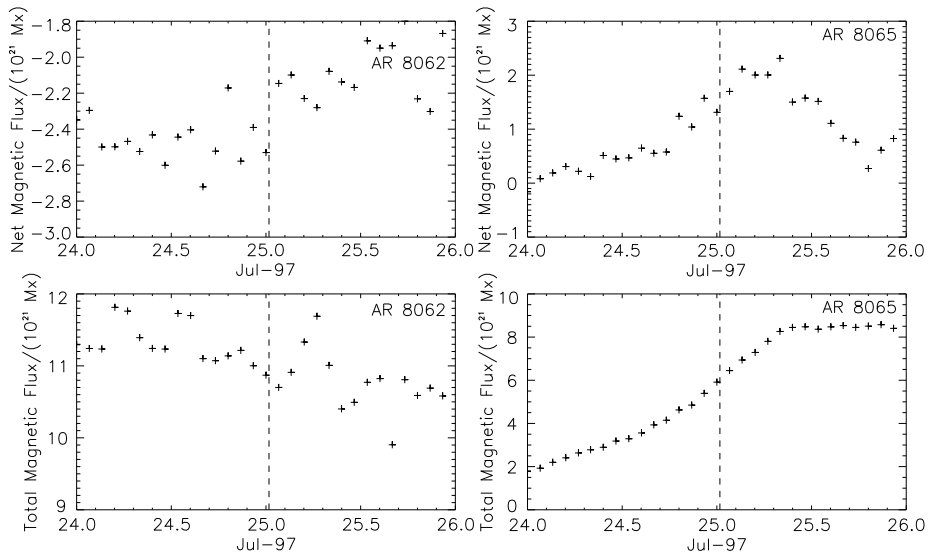
Figure 7 Variation of magnetic flux in AR 8062 and AR 8065 during the process of the HIL formation, the dashed line indicates the moment that the HIL formed. Left panel: variations of AR 8062 for net magnetic flux and total magnetic flux; Right panel: variations of flux in AR 8065.

was formed at 00:24 on 25 July. AR 8065 is a new β-type active region. AR 8062 appeared in the east limb on 17 July. It was an α-type active region originally; later, on 25 July, it became a β-type active region.

Variations of magnetic flux in AR 8062 and AR 8065 are shown in Figure 7; the interval from the left to the dashed line for each plot is the formation period. The flux variation of AR 8062 is plotted in the left panel; the right panel shows the variation of the flux in AR 8065. For AR 8065, we can see both the total magnetic flux and net magnetic flux are increasing during the formation period. The net magnetic flux of AR 8065 is positive and increasing, the positive magnetic polarity dominates the active region. For AR 8062, the negative magnetic polarity dominates the active region. When we calculate the magnetic flux in AR 8062, the southeast region is also considered as part of this active region. Looking at the HIL carefully, we are not sure whether this part contributes to the system. If we cut this part out, the net magnetic flux will be changed to be positive; then the positive magnetic flux dominates the two regions connected by the HIL.

3.1.3. Case 3

Figure 8 displays a transequatorial loop on 20 April 2000. The left panel is a soft X-ray image; the right panel is the corresponding full-disk magnetogram. The TL connects the positive polarity around AR 8963 in the northern hemisphere and the negative polarity in AR 8968 in the southern hemisphere.

Formation of the TL and evolution of related active regions are demonstrated in Figure 9. SXT images are shown in the top panel: there is no clear TL in the left image at 14:58 on 19 April, an entire TL appeared at 15:02 on 20 April firstly. In the middle and bottom panels, the corresponding magnetograms of AR 8968 and AR 8963 are shown. AR 8963 is an old active region and AR 8968 is a new active region, both are $\beta\gamma$-type active regions.
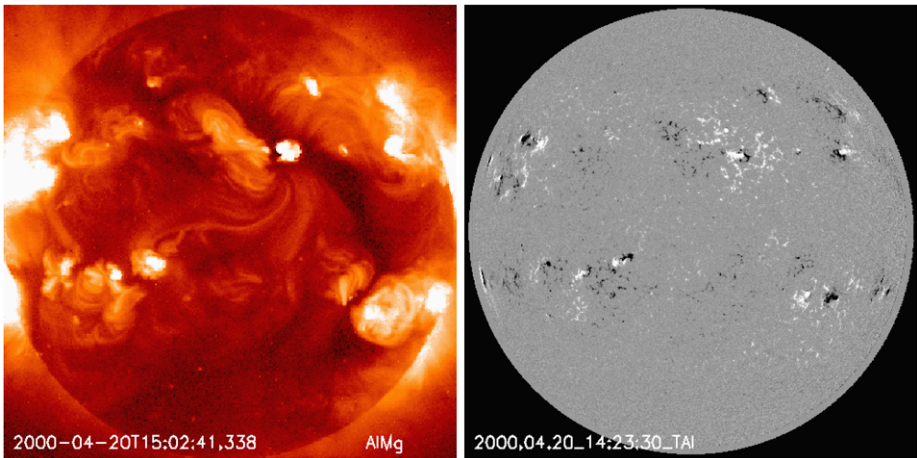
Figure 8 A transequatorial loop between AR 8963 and new active region AR 8968 on 20 April 2000. Left: a coronal image from *Yohkoh*/SXT; Right: a photospheric longitudinal magnetogram from SOHO/MDI.
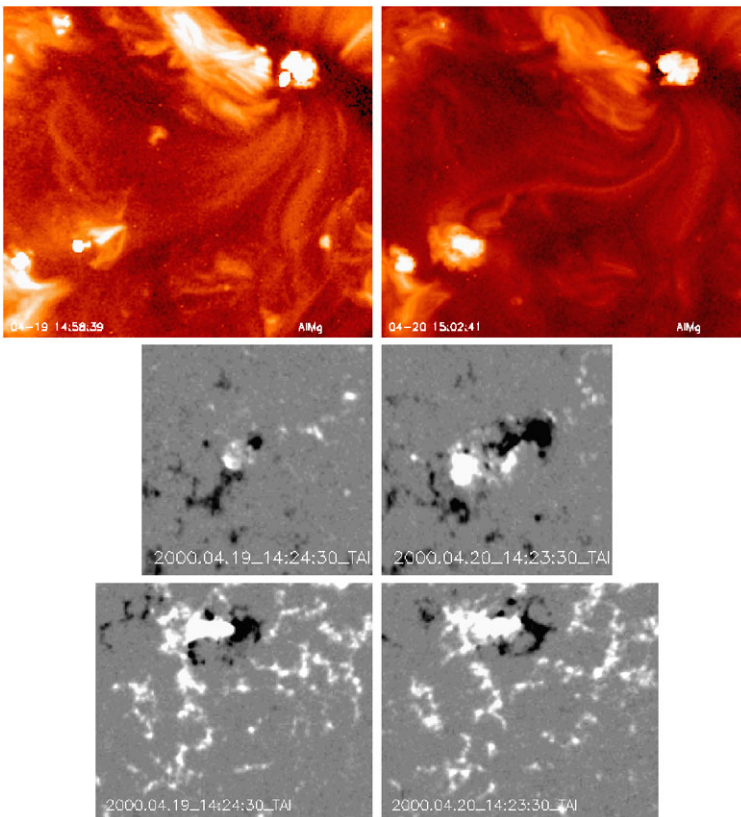

Figure 9 Formation of a transequatorial loop between AR 8963 and new active region AR 8968 during the period from 19 April 2000 to 21 April 2000. Top: formation of the TL, the field of view is 200 pixel × 180 pixel, 1 pixel = 4.91$''$; Middle: evolution of AR 8968, the field of view is 100$''$ × 100$''$; Bottom: evolution of AR 8963; the field of view is 140$''$ × 120$''$.
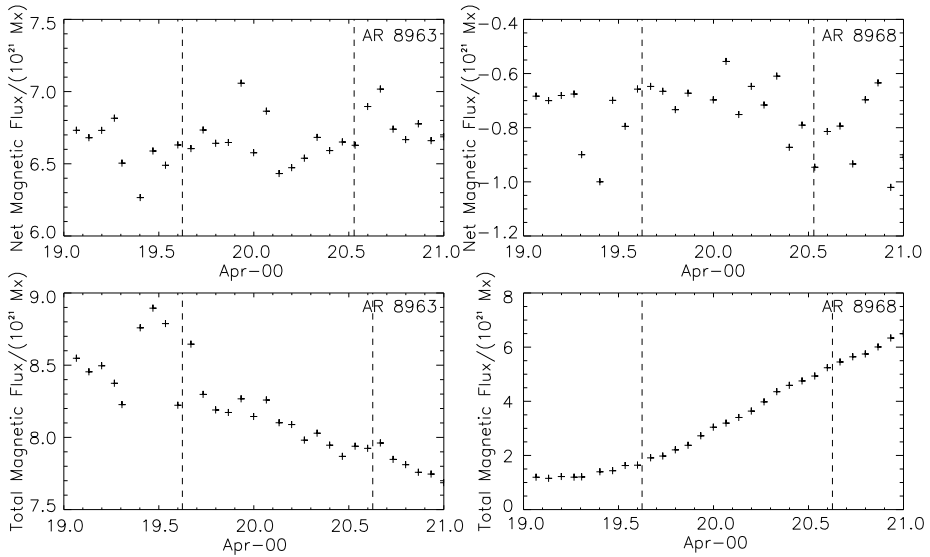
Figure 10 Variations of the magnetic flux in AR 8963 and AR 8968 during the process of formation of the TL, the interval in the dashed lines is the period of TL formation. The left panel shows the variation of the AR 8963 for net magnetic flux and total magnetic flux; in the right panel, variation of the magnetic flux in AR 8968 is shown.

Figure 10 shows variation of magnetic flux; the interval between the dashed lines in each plot is the formation period. For AR 8968, the total magnetic flux is increasing during the formation of TL, it is in the increasing phase. For AR 8963, the total magnetic flux is decreasing, which means that AR 8963 is in the decaying phase. For AR 8968, the net magnetic flux is negative. For AR 8963, the net magnetic is positive. So the negative magnetic polarity has a preference in AR 8968; the positive magnetic polarity has a preference in AR 8963.

3.1.4. Case 4

Figure 11 displays another TL appearing on 7 July 1999. The left panel is a coronal image observed by the soft X-ray telescope; the right panel is a full-disk longitudinal magnetogram. The TL connects the positive polarity in AR 8614 in the northern hemisphere and the negative polarity in AR 8626 in the southern hemisphere.

Figure 12 shows the formation of the TL and the evolution of related active regions. The top panel shows the formation of the TL through soft X-ray images. The TL formed at 06:16 on 7 July originally; then it became wider and brighter, at 12:41 on 7 July, it was formed completely. In the middle and bottom of the panel, we show the evolution of AR 8626 and AR 8614. For SOHO/MDI magnetograms, at 12:51 on 7 July, the data have problems in the northern hemisphere, so the magnetogram for AR 8614 is not presented. Both of them are complex $\beta\gamma$-type active regions, AR 8614 is an old region and AR 8626 is a new region.

Figure 13 plots variations of magnetic flux in the two active regions. The dotted lines show the appearance of weak transequatorial structures, and the interval between the dashed lines is the TL formation period. For AR 8626, the total magnetic field is increasing during the period of formation. For AR 8614, the total magnetic field is decreasing. For AR 8626, the net magnetic flux is negative, and it is smaller in absolute value. It shows that the negative
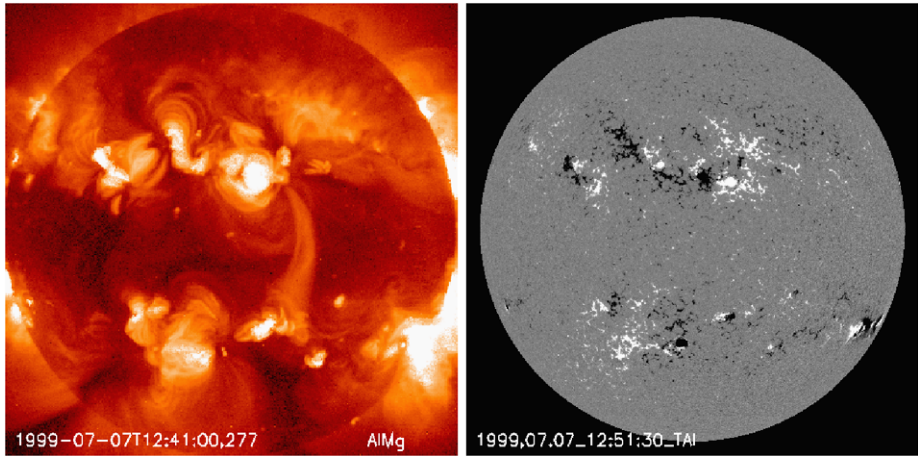
Figure 11 A transequatorial loop (TL) appeared on 7 July 1999. Left: *Yohkoh*/SXT image; Right: SOHO/MDI image.
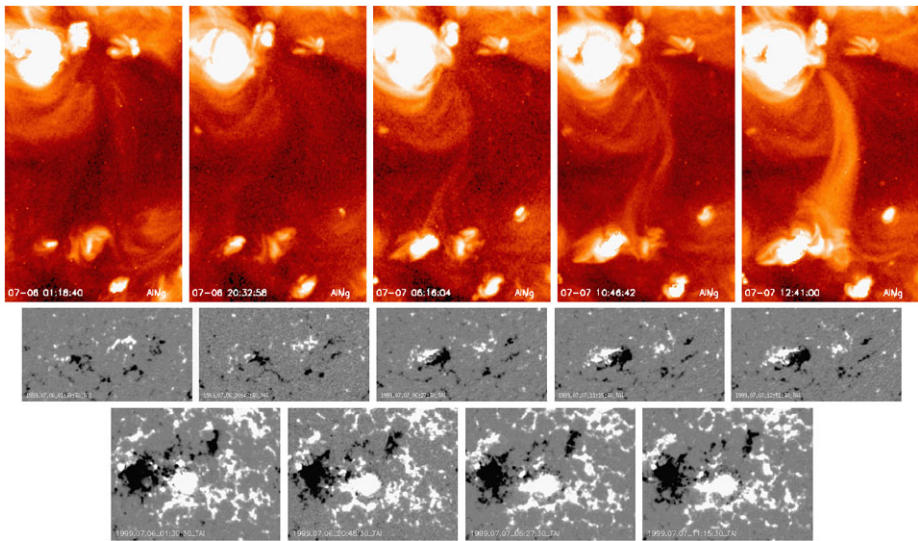

Figure 12 Top: formation of a transequatorial loop between AR8614 (N) and new active region AR8626 (S) from 6 July 1999 to 8 July 1999, the field of view is 120 pixel × 200 pixel, 1 pixels = 4.91″; Middle: evolution of AR 8626, the field of view is 180″ × 100″; Bottom: evolution of AR 8614; the field of view is 180″ × 140″.

magnetic polarity is favored and the negative flux increases more quickly than the positive flux. For AR 8614, the net magnetic flux is positive and it has a tendency of decreasing. It shows the positive magnetic polarity has a preference.

3.1.5. Results and Discussion

By investigating the magnetic properties of active regions related with the four interconnecting loops, we found that an interconnecting loop will not form immediately after the birth
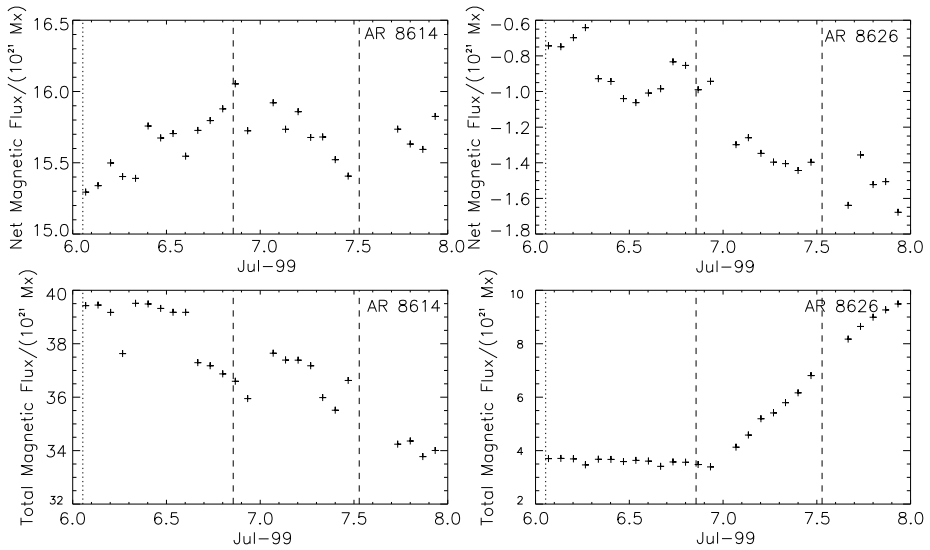
Figure 13 Variations of magnetic flux in AR 8614 and AR 8626. Left panel shows the variation of net magnetic flux and total magnetic flux in AR 8614; right panel shows the variation of magnetic flux in AR 8626. The dotted lines show the appearance of the transequatorial loop, and the interval between the dashed lines shows the formation period of the TL.

of a new active region. Only after the magnetic flux arrived at a certain threshold, will the IL be generated. The formation types of two hemispheric interconnecting loops (HILs) and two transequatorial loops (TLs) are diverse.

For the HIL generated on 21 May 1997, firstly, a faint, narrow interconnecting loop was formed, later the loop became wider and brighter. Both of the active regions are simplified β-type magnetic types, they are in the same increasing phases and the same polarity dominates in the two active regions.

For this HIL it is possible that the magnetic-field lines existed prior to the brightening. They cannot be observed earlier due to the low intensity. The newly emerging flux from AR 8045 contributes magnetic energy. The gradual growth in brightness could be explained by progressive heating, or progressive filling up, of the loop with plasma from the new region. The density and temperature increase, the intensity increases, and the HIL became brighter and wider.

The latitudinal positions of the two active regions are almost identical. During the brightening of HIL, the total magnetic fluxes of the two active regions are increasing. This may be because they belong to the same toroidal field; AR 8040 emerged firstly, then AR 8045 emerged.

Considering the HIL on 25 July 1997, the wide and bright structures expanded from each of the two regions separately. Then it became a distinct, complete loop rooted in two active regions. The formation of this loop may be due to the magnetic reconnection of the two active regions. From Figure 6 we can see that there are small loops originating from the positive polarity of AR 8062. With the growth of AR 8065, there are small loops anchored from the negative magnetic polarity of AR 8065. It is possible that the differential rotation drives magnetic reconnection which induces the loop formation between the positive polarity of AR 8062 and the negative polarity of AR 8065.

Both of the active regions are simple magnetic types (α- and β-type). AR 8065 is in the increasing phase and AR 8062 is in the decaying phase. The net magnetic fluxes of the two active regions are opposite. This could be explained as the magnetic-flux imbalance between the two active regions produces a chance of creating an interconnecting loop.

The TL on 20 May 2000 was a diffuse structure at the beginning, then a clear, narrow, twisted TL formed. The TL existed more than one day before it disappeared. The brightening of the twisted loop may be because the loop existed in the sub-photosphere; during the emergence of new magnetic flux, the loop emerged with the new active region. After one day, it cooled down and disappeared.

Considering the TL on 7 July 1999, at the initial stage, there was a diffuse structure; about twenty hours later, the diffuse structure changed to a faint loop shape; after that the loop shape became sharp and clear, then the structure became wider, and finally the whole vivid TL was generated. During the birth of this TL, the magnetic loop of this TL may have existed previously. With the injection of energy, the plasma density and temperature increase, and then a distinct loop can be seen.

The formation of several types of interconnecting loop is demonstrated in these events: the IL emerges from sub-photosphere; the IL is created from magnetic reconnection; the magnetic flux tube already existed; when the plasma is filled, it can be observed.

3.2. Statistical Results

Statistical results for 50 ILs are shown in Table 3. Thirty-five HILs and 15 TLs are included. The properties for these ILs are presented in this table. For 35 HILs, eighteen old active regions, the values of Φ_{tot} are increasing; for six old active regions, the values of Φ_{tot} are decreasing. For 15 TLs, ten old active regions, the values of Φ_{tot} are increasing; four old active regions, the values of Φ_{tot} are decreasing. Among the 35 HILs, there are 21 HILs, the signs of Φ_{net} are opposite for the two active regions; among the 15 TLs, there are 11 TLs, the signs of Φ_{net} are opposite for the two active regions. This could be because the ratio of number of AR pairs within a certain range of separation is higher than that on the Equator.

Thirty-five HILs and only 15 TLs are found in this study: HILs appear more frequently than TLs. We have already described the values of Φ_{tot} which are increasing for all of the newly born active regions in the first paragraph of this section. For old active regions, both for the HILs and TLs, for more than half of the regions, the values of Φ_{tot} are increasing. If we consider the two active regions connected by one IL as a magnetic-flux system, it is the

Table 3 50 interconnecting loops (ILs).

IL (50)									
HIL[a] (35)					TL[b] (15)				
Φ_{tot}			Φ_{net}		Φ_{tot}			Φ_{net}	
↑	↓	?	S[c]	O[d]	↑	↓	?	S	O
18	6	11	14	21	10	4	1	4	11

[a]Hemispheric interconnecting loop.

[b]Transequatorial loop.

[c]The signs of Φ_{net} are same for two active regions connected by IL.

[d]The signs of Φ_{net} are opposite for two active regions connected by IL.

same for both HIL and TL: the total magnetic flux of the system has a tendency of increasing. Originally, we thought it might be caused by the two active regions connected by a HIL which are close in latitude, and two active regions related with TL are close in longitude. Then we analyzed the positions of these active regions. We did not find the difference in latitudine to be smaller for the increasing old active regions than the decreasing old active regions in HIL, and we did not find the difference in longitudine to be smaller for the increasing old active regions than the decreasing old active regions in TLs. This result could be explained as a new active region inducing the generation of an IL; then the IL acts as a tunnel to transport plasma from the new one to the old.

If we consider the signs of Φ_{net}, more than half of the cases are opposite for HIL, and the probability is a little higher for TL. This confirms that the sum of the net magnetic flux for the IL system has a tendency to zero. It means that there is a high probability of creating an IL, when the signs of net magnetic flux of active regions are opposite. If the active regions connected by these IL are also related to other ILs, there is a high possibility for them to be of the same sign as regards Φ_{net}. Active-region pairs with opposite net magnetic flux signs have a higher ratio for TLs than ILs, which may be explained as the net magnetic flux being opposite for the different hemispheres.

4. Conclusion

New active regions with emerging magnetic flux induce the formation of interconnecting loops (ILs). Fifty cases are found in around five years. It is a common phenomenon that a new active region plays a role in generating ILs. There are 35 same-hemisphere interconnecting loops (HILs) and 15 transequatorial loops (TLs) in these ILs. Thirty-five HILs and 15 TLs shows that the HILs appear more frequently than TLs.

The formation processes of four ILs are analyzed in detail. The formation is different in each of the ILs. The variation of the total magnetic flux and the values of the net magnetic flux are plotted.

If we consider the two active regions connected by one IL as a magnetic system, the total magnetic flux of this system has a tendency of increasing. This is the same for both HIL and TL. In more than a half of the cases, the signs of the net magnetic flux are opposite for the two active regions, no matter whether it is HIL or TL. From this point of view, there is no difference between HILs and TLs.

References

Chase, R.C., Krieger, A.S., Svestka, Z., Vaiana, G.S.: 1976, In: *Space Research XVI: Proc. of the Open Meetings of the Working Groups on Physical Sciences and Symposium and Workshop Results from Coodinated Upper Atmosphere Measurement Programmes*, Akademie-Verlag, Berlin, 917.

Choudhary, D.P., Venkatakrishnan, P., Gosain, S.: 2002, *Astrophys. J.* **573**, 851.

Feynman, J., Martin, S.F.: 1995, *J. Geophys. Res.* **100**, 3355.

Fárník, M., Karlický, M., Švestka, Z.: 1999, *Solar Phys.* **187**, 33.

Green, L.M., Démoulin, P., Mandrini, C.H., van Driel-Gesztelyi, L.: 2003, *Solar Phys.* **215**, 307.

Harra, L., Crooker, N., Mandrini, C., van Driel-Gesztelyi, L., Dasso, S., Wang, J., Elliott, H., Attrill, G., Jackson, B., Bisi, M.: 2007, *Solar Phys.* **244**, 95.

Howard, R.F., Harvey, J.W., Forgach, S.: 1990, *Solar Phys.* **130**, 295.

Jiang, J., Choudhary, A.R., Wang, J.: 2007, *Solar Phys.* **245**, 19.

Khan, J., Hudson, H.: 2000, *Geophys. Res. Lett.* **27**, 1083.

Lara, A., Gopalswamy, N., DeForest, C.: 2000, *Geophys. Res. Lett.* **27**, 1435.

Martin, S.F., Dezso, L., Antolova, A., Kucera, A., Harvey, K.L.: 1982, *Adv. Space Res.* **2**, 39.

Pevtsov, A.: 2000, *Astrophys. J.* **531**, 553.

Scherrer, P.H., Bogart, R.S., Bush, R.I., Hoeksema, J.T., Kosovichev, A.G., Schou, J., *et al.*: 1995, *Solar Phys.* **162**, 129.

Švestka, Z., Howard, R.: 1981, *Solar Phys.* **71**, 349.

Tsuneta, S.: 1996, *Astrophys. J. Lett.* **456**, L63.

Tsuneta, S., Acton, L., Bruner, M., Lemen, J., Brown, W., Caravalho, R., Catura, R., Freeland, S., Jurcevich, B., Owens, J.: 1991, *Solar Phys.* **136**, 37.

Yokoyama, M., Masuda, S.: 2009, *Solar Phys.* **254**, 285.

Wang, J., Zhou, G., Wen, Y., Zhang, Y., Wang, H., Zhang, J., Harra, L.: 2006, *Chin. J. Astron. Astrophys.* **6**, 247.

Wang, J., Zhang, Y., Zhou, G., Harra, L., Williams, D., Jiang, Y.: 2007, *Solar Phys.* **244**, 75.

Zhang, Y., Zhang, M., Zhang, H.Q.: 2008, *Solar Phys.* **250**, 75.